Chemistry & Biodiversity

WILEY-VCH

CHEMISTRY & BIODIVERSITY

RESEARCH ARTICLE

Synthesis and Evaluation of the Antibacterial Activity of *N*-Substituted Piperazine Flavonol Derivatives

Jin Wang[1] | Xin-Ming Li[2] | Si-Jiao Cui[3] | Jia-Xin Liu[2] | Chi-Yu Sun[1] | Li-Li Sui[1] | Da-Jun Zhang[1] | Tian Luan[1]

[1]School of Pharmacy, Shenyang Medical College, Shenyang, China | [2]School of Basic Medicine, Shenyang Medical College, Shenyang, China | [3]Shenyang Food and Drug Inspection Institute, Shenyang, China

Correspondence: Da-Jun Zhang (zhangdajun2008@126.com) | Tian Luan (luantian@symc.edu.cn)

Received: 21 January 2025 | **Revised:** 3 May 2025 | **Accepted:** 16 June 2025

Funding: This study received funding from the Scientific Research Project of the Department of Education of Liaoning Province, China (No. JYTMS20231407) and the Project of Science and Technology Department of Liaoning Province, China (No. 2024-MS-226; No. 2023-MS-328).

Keywords: antibacterial activity | biofilm inhibition | flavonol | molecular docking | piperazine | staphylococcal accessory regulator

ABSTRACT

Diseases resulting from bacterial invasion have consistently posed a substantial threat to public health and safety. To address this problem, this study aimed to discover novel chemical structures with antibacterial activity by using flavonols as lead compounds. Through structural modifications, we introduced various *N*-substituted piperazine compounds to synthesize ten previously unreported compounds. Subsequently, the antibacterial activities of these compounds against *Staphylococcus aureus* and *Escherichia coli* were evaluated. Compound **2g** was identified as the most potent compound, exhibiting minimum inhibitory concentration (MIC) values of 6.25 μg/mL against *S. aureus* and 25 μg/mL against *E. coli*. Additionally, compound **2g** effectively inhibited the growth of *S. aureus* and *E. coli*, with inhibition zones measuring 16 mm and 15 mm, respectively. At a concentration of 8 × MIC, the bacterial counts of both strains were reduced by 1.75 and 0.72 logCFU/mL within 60 min. Furthermore, compound **2g** significantly inhibited the formation of *S. aureus* biofilms. Molecular docking studies suggested that the staphylococcal accessory regulator might be its potential target. This study provides valuable insights into the antibacterial activity of flavonoids and offers a scientific foundation for the development of novel antibacterial agents.

1 | Introduction

For a long time, infectious diseases caused by bacterial invasion have been posing a huge threat to public health and safety. A large amount of clinical data indicates that *Escherichia coli*, *Staphylococcus aureus*, *Klebsiella pneumoniae*, *Acinetobacter baumannii*, and *Pseudomonas aeruginosa* are common pathogenic bacteria [1]. Meanwhile, the incidence of multi-drug-resistant bacteria worldwide is constantly increasing, which makes the treatment of bacterial infections even more challenging. Therefore, there is currently an urgent need to identify novel scaffolds with potent antibacterial activity. In recent years, researchers have discovered numerous antibacterial compounds featuring heterocyclic scaffolds [2–6]. Among them, flavonoids are naturally present in many plants and possess a wealth of pharmacological activities, including antibacterial [6], anti-aging [7, 8], antioxidant [9], antiviral [10, 11], and central nervous system regulatory properties [12]. More and more research is being carried out in this field, and researchers are exploring its antibacterial mechanisms from multiple perspectives. The antibacterial mechanisms mediated by flavonoids mainly include interfering with the synthesis of bacterial nucleic acids [13, 14], damaging the bacterial cell

Jin Wang, Xin-Ming Li, and Si-Jiao Cui contributed equally to this work.

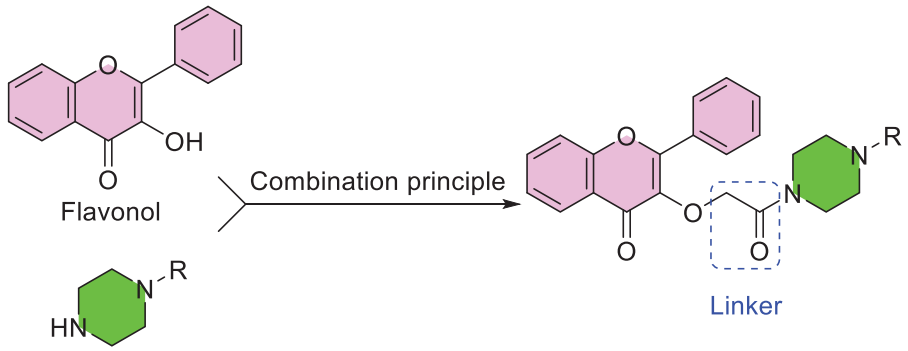

FIGURE 1 | Design of target compounds based on the structure combination principle.

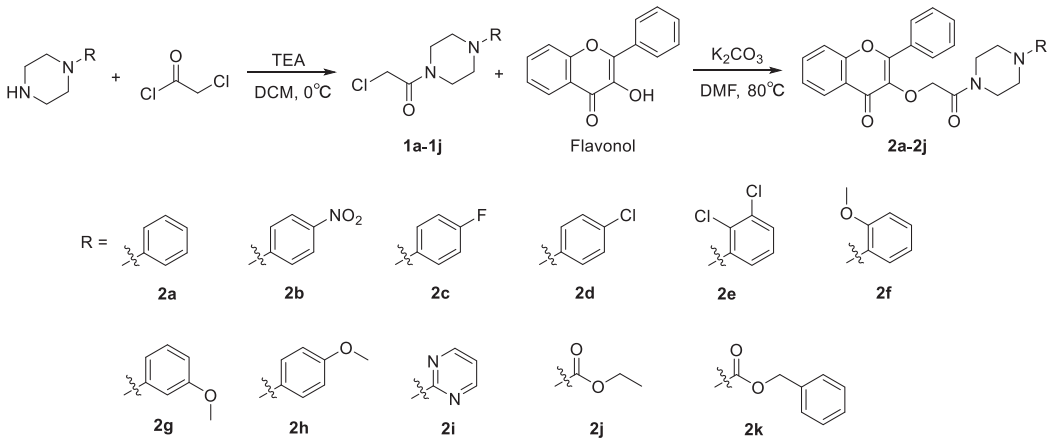

SCHEME 1 | Synthetic route of target compounds.

membrane [15, 16], and inhibiting energy metabolism [17, 18]. Additionally, studies have found that flavonoids exhibit broad-spectrum antibacterial effects [19].

In the field of medicinal chemistry, piperazine is a basic nitrogen-containing heterocyclic compound with natural biological activity and is a high-quality active fragment widely used for structural modification. According to the data on drugs containing piperazine compounds approved by the U.S. Food and Drug Administration (FDA), most of these compounds are *N*-acyl or *N*-aryl piperazines, such as those containing phenyl, benzyl, methyl, or carboxylic acid groups [20]. Piperazine can interact with certain biological target molecules through hydrogen bonds or ionic bonds by using its nitrogen atom as a hydrogen bond acceptor or undergoing ionization under physiological conditions, thereby exerting its pharmacological effects [21–23]. Meanwhile, it can enhance the water solubility of lead compounds and serve as a good splicing fragment in drug design. In addition, acyl functional groups play a crucial role in many bioactive molecules. During the optimization of lead compounds, they can maintain or enhance the activity, selectivity, and pharmacokinetic properties of these compounds [24].

The aforementioned findings have piqued our interest in utilizing 3-hydroxyflavone (Flavonol) as a lead compound and incorporating acylated piperazine moieties into its scaffold (Figure 1), with the objective of enhancing the antibacterial efficacy of flavonols and offering novel insights for the development of innovative flavonoid-based antibacterial agents.

2 | Results and Discussion

2.1 | Chemistry

Scheme 1 shows the procedure adopted to obtain the target compounds. Intermediates **1a–1k** were synthesized according to the procedure outlined in the reference [25]. The final products **2a–2k** were obtained via nucleophilic substitution reactions of the corresponding intermediates using potassium carbonate as the base in *N*, *N*-dimethylformamide at 80°C. This method yielded good to excellent results (67-89%). Before biological evaluation, all target compounds were characterized via mass spectrum, ^{1}H-NMR, and ^{13}C-NMR.

2.2 | The Minimum Inhibitory Concentration of the Target Compounds and Their Preliminary Structure–Activity Relationship

S. aureus is a Gram-positive bacterium, and *E. coli* is a Gram-negative bacterium. Since levofloxacin is the most widely prescribed quinolone antibacterial drug in clinical practice and exhibits highly favorable antibacterial activity, it was selected as the positive control drug. Meanwhile, flavonol was used as the parent compound for reference in this experiment. The minimum inhibitory concentration (MIC) values of all compounds against the above two bacteria are shown in Table 1. The antibacterial activity of flavonol against *S. aureus* and *E. coli* is relatively weak, with MIC values exceeding 100 μg/mL. In contrast, levofloxacin

TABLE 1 | The minimum inhibitory concentration (MIC) values of the target compounds.

Comp.	MIC, μg/mL	
	S. aureus ATCC29213	*E. coli* ATCC25922
2a	>100	>100
2b	>100	>100
2c	>100	50 ± 2.12
2d	>100	>100
2e	>100	>100
2f	12.5 ± 0.89	50 ± 2.46
2g	6.25 ± 0.26	25 ± 0.14
2h	>100	>100
2i	>100	>100
2j	>100	>100
2k	>100	>100
Flavonol	>100	>100
Levofloxacin	0.195 ± 0.03	0.195 ± 0.02

TABLE 2 | Cytotoxicity of compounds **2f** and **2g**.

Comp.	IC_{50}, μM
	L02
2f	>100
2g	>100

exhibits potent activity against both bacteria, with MIC values of 0.195 μg/mL. Among the 11 compounds synthesized in this experiment, although their antibacterial activity did not exceed that of levofloxacin, three compounds showed better antibacterial activity against the above two bacteria compared to flavonol. Notably, the inhibitory activity of compounds **2f** and **2g** against *S. aureus* was significantly enhanced, with MIC values of 12.5 and 6.25 μg/mL, respectively, which were 8 and 16 times lower than that of the lead compound. The MIC values of compounds **2c**, **2f**, and **2g** against *E. coli* were 50, 50, and 25 μg/mL, respectively, with compound **2g** demonstrating the most potent antibacterial activity. The preliminary structure-activity relationship (SAR) analysis revealed that introducing a benzene ring on the piperazine moiety and substituting electron-donating groups at the ortho or meta positions of the benzene ring significantly enhanced antibacterial activity. Notably, meta-substitution resulted in higher activity compared to ortho-substitution.

2.3 | Cytotoxicity

Given that the antibacterial activities of compounds **2f** and **2g** were significantly enhanced compared to flavonol, their cytotoxicity against L02 human normal hepatocytes was evaluated using the MTT assay in this study. As shown in Table 2, the IC_{50} values of both compounds against L02 cells exceeded 100 μM, suggesting that these compounds exhibit potent antibacterial activity while maintaining low cytotoxicity.

2.4 | The Antibacterial Efficacy of Compound 2g Was Assessed Using the Oxford Cup Method

Since compound **2g** exhibited the strongest antibacterial activity among all the compounds, it was selected as the representative compound for further in-depth study of its antibacterial activity. First, levofloxacin was used as a positive control to evaluate the antibacterial efficacy of compound **2g** using the Oxford cup method. The results are presented in Figure 2. An inhibition zone with a diameter of 16 mm was observed around the Oxford cup containing compound **2g** at a concentration of 8 × MIC, indicating its significant inhibitory effect on *S. aureus* growth. Similarly, an inhibition zone of 15 mm was observed against *E. coli*, demonstrating that compound **2g** also effectively inhibited the growth and reproduction of this bacterium (Figure 3).

2.5 | The Time-kill Curve of Compound 2g

The time-kill curve can help researchers accurately analyze the effectiveness of the bactericide. To further evaluate the bactericidal potential of the synthesized flavonoid derivatives, a time-kill kinetics experiment was conducted to investigate the inhibitory and bactericidal effects of compound **2g** on *S. aureus* and *E. coli*. The experimental results presented in Figure 4 demonstrate that at a concentration of 8 × MIC for compound **2g**, the initial population of *S. aureus* decreased by 1.75 logCFU/mL within the first hour and by 2.29 logCFU/mL after 24 h, with no regrowth observed during this period. Similarly, the initial population of *E. coli* decreased by 0.72 logCFU/mL within the first hour and by 1.70 logCFU/mL after 24 h, with no regrowth detected within 24 h.

2.6 | The Effect of Compound 2g on *S. aureus* Biofilm

Since compound **2g** demonstrated superior antibacterial activity against *S. aureus*, this study further explored the impact of compound **2g** on the formation of *S. aureus* biofilms. The experimental results presented in **Figure 5** demonstrate that the biofilm quantity of *S. aureus* in the control group increased over time. In contrast, the biofilm formation in the compound **2g** treatment group was significantly lower at all time points compared to the control group ($p < 0.001$). These findings suggest that compound **2g** effectively inhibits the formation of *S. aureus* biofilms.

2.7 | Molecular Docking and Molecular Dynamic Simulation Analysis

The staphylococcal accessory regulator (SarA) serves as a pivotal regulatory component that governs the expression of *S. aureus* virulence factors and has been recognized as indispensable for biofilm formation [26]. Since our previous experiments demonstrated that compound **2g** significantly inhibits the formation of *S. aureus* biofilms, we hypothesized in this study that SarA is

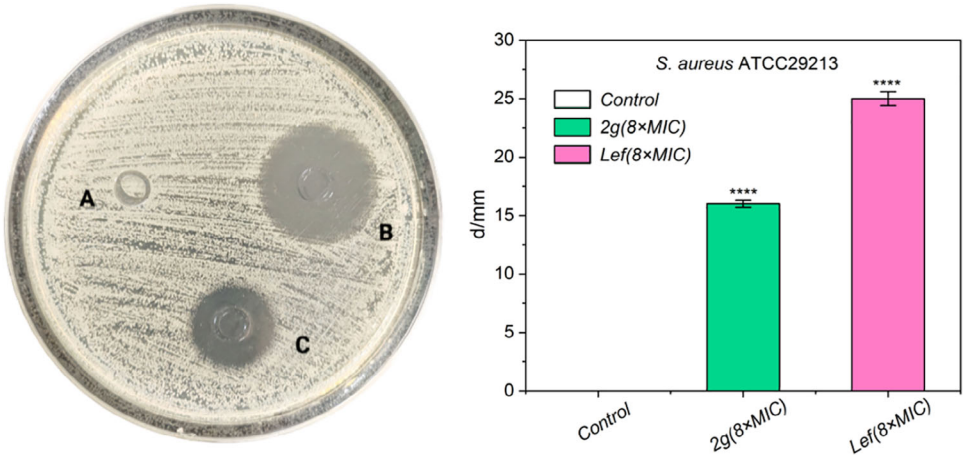

FIGURE 2 | Growth of *S. aureus* after treatment with compound **2g** and levofloxacin (In the left image, A is the control group, B is the levofloxacin treatment group, and C is the compound **2g** treatment group). ****$p < 0.0001$ ($n = 3$).

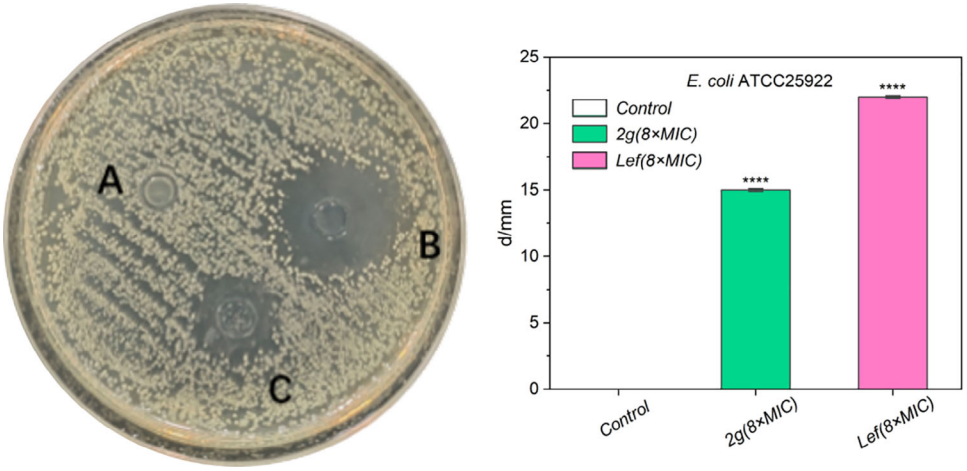

FIGURE 3 | Growth of *E. coli* after treatment with compound **2g** and levofloxacin (In the left image, A is the control group, B is the levofloxacin treatment group, and C is the compound **2g** treatment group). ****$p < 0.0001$ ($n = 3$).

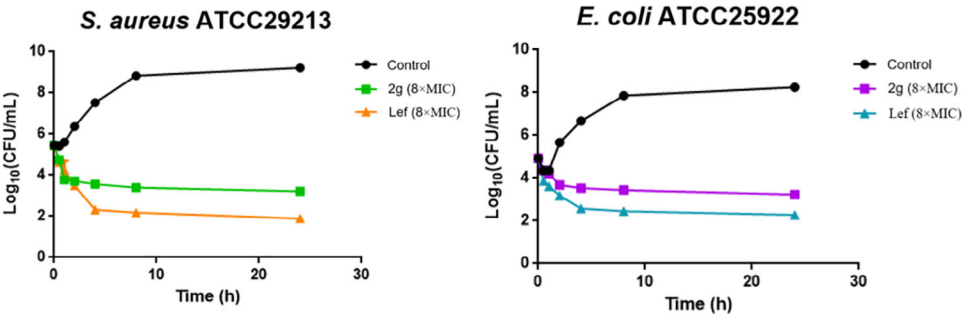

FIGURE 4 | The time-kill kinetics of compound **2g** against two bacterial strains.

a potential target of compound **2g**. To elucidate the structural mechanism of action, molecular docking analysis was performed, providing insights for identifying targets of similar compounds. The experimental results are shown in Figure 6. The oxygen atom at position 1 of the flavonol scaffold can act as a hydrogen bond acceptor, forming a hydrogen bond with the hydroxyl hydrogen atom of Ser114 in subunit A. Meanwhile, the methoxy group at the meta position of the *N*-substituted phenyl side chain can also serve as a hydrogen bond acceptor, forming an additional hydrogen bond with the amino hydrogen atom of Asn161 in subunit B. This result, to some extent, elucidates the reason for the ideal antibacterial activity observed when a methoxy group is introduced at the meta position of the benzene ring. In addition, the piperazine moiety forms a carbon-hydrogen

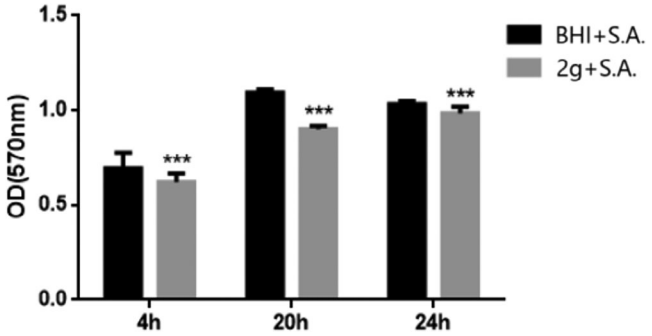

FIGURE 5 | Inhibitory effect of compound **2g** on *S. aureus* biofilm formation. ***$p < 0.001$ ($n = 3$).

bond with the His159 residue of subunit B. Furthermore, the flavonol scaffold engages in multiple interactions with various amino acid residues through diverse intermolecular forces. The LibDockScore is 92.3068 and the AbsoluteEnergy is 83.1059. These results indicate that compound **2g** exhibits a strong binding affinity for SarA and thus has the potential to act as a SarA inhibitor.

To evaluate the stability of the 2FRH-**2g** docked complex, a molecular dynamics simulation experiment was conducted on the 2FRH-**2g** docked complex. The experimental results are shown in **Figure 7**. The root-mean-square deviation (RMSD) value remained within the range of 0.63 to 2.27 Å throughout the 1000 ps simulation, with an average of 1.65 ± 0.29 Å. These results indicate that the complex exhibited relatively high stability throughout the simulation process.

3 | Conclusions

In this study, 11 novel flavonoid derivatives were synthesized using flavonol as the lead compound. Their structural characterization and antibacterial efficacy were thoroughly evaluated. The results demonstrated that flavonol modified with an *N*-substituted piperazine group exhibited superior antibacterial activity against *S. aureus* and *E. coli*. Notably, compound **2g** achieved an MIC of 6.25 μg/mL and also showed significant inhibition of *S. aureus* biofilm formation. Molecular docking studies suggested that SarA might be the target responsible for this biofilm inhibition. These findings provide valuable insights and directions for the development of novel flavonoid-based antibacterial agents, offering experimental data to support potential future clinical applications.

4 | Experimental

4.1 | Synthesis of Compounds 2a–2k

In a 100 mL round-bottomed flask, sequentially add flavonol (5 mmol, 1.1912 g), anhydrous potassium carbonate (15 mmol, 2.0731 g), and *N*, *N*-dimethylformamide (DMF, 20 mL). Stir the reaction mixture at room temperature for 1 hour. Separately, measure 10 mL of DMF and transfer it to a beaker to dissolve the intermediates (**1a**–**1k**, 6 mmol). Transfer this solution to a constant pressure-dropping funnel and slowly drip it into the reaction flask at a constant rate. Upon completion of dripping, gradually increase the temperature to 80°C and continue stirring for 6 h. Monitor the reaction progress using thin-layer chromatography (TLC) until completion. Once the reaction is complete, cool the mixture to room temperature and pour it into a beaker containing 100 mL of cold water. Filter the precipitated solids under suction. The collected solid is purified by column chromatography using a dichloromethane/methanol (20:1) eluent to yield the final products **2a**–**2k**.

4.2 | 3-(2-Oxo-2-(4-Phenylpiperazin-1-Yl)Ethoxy)-2-Phenyl-4*H*-Chromen-4-One (2a)

White solid, yield 72.7%, melting point (m.p.) 138.4–139.6°C, ^{1}H-NMR (400 MHz, DMSO-d_6): δ 8.14 (d, J = 15.7 Hz, 3H), 7.90-7.75 (m, 2H), 7.57 (d, J = 5.3 Hz, 3H), 7.52 (t, J = 7.4 Hz, 1H), 7.23 (t, J = 7.7 Hz, 2H), 6.94 (d, J = 8.1 Hz, 2H), 6.81 (t, J = 7.3 Hz, 1H), 4.97 (s, 2H), 3.55 (d, J = 5.2 Hz, 4H), 3.10 (d, J = 5.4 Hz, 4H); ^{13}C-NMR (101 MHz, DMSO-d_6): δ 173.79, 165.68, 154.67, 154.64, 150.69, 139.23, 134.15, 130.87, 130.45, 128.94 (2C), 128.64 (2C), 128.51 (2C), 125.12, 124.90, 123.33, 119.31, 118.40, 115.85 (2C), 69.06, 48.47, 48.18, 44.08, 40.90; ESI-MS *m/z*: Anal. Calcd. for $C_{27}H_{25}N_2O_4^+$ [M + H]$^+$(441.18), Found: 441.17.

4.3 | 3-(2-(4-(4-Nitrophenyl)Piperazin-1-Yl)-2-Oxoethoxy)-2-Phenyl-4*H*-Chromen-4-One (2b)

Yellow solid, yield 67.2%, m.p. 173.4–174.3°C, ^{1}H-NMR (400 MHz, DMSO-d_6): δ 8.21–8.11 (m, 3H), 8.11–8.04 (m, 2H), 7.91–7.77 (m, 2H), 7.64–7.49 (m, 4H), 7.03 (d, J = 9.5 Hz, 2H), 5.00 (s, 2H), 3.67–3.59 (m, 3H), 3.59–3.50 (m, 4H), 3.50 (s, 1H); ^{13}C-NMR (101 MHz, DMSO-d_6): δ 173.78, 166.00, 154.68, 154.63, 154.25, 139.21, 136.96, 134.15, 130.88, 130.43, 128.63 (2C), 128.51 (2C), 125.66 (2C), 125.12, 124.89, 123.31, 118.39, 112.52 (2C), 69.05, 45.95, 45.64, 43.34, 40.46; ESI-MS *m/z*: Anal. Calcd. for $C_{27}H_{24}N_3O_6^+$ [M + H]$^+$(486.17), Found: 486.16.

4.4 | 3-(2-(4-(4-Fluorophenyl)Piperazin-1-Yl)-2-Oxoethoxy)-2-Phenyl-4*H*-Chromen-4-One (2c)

White solid, yield 82.9%, m.p. 138.5–139.1°C, ^{1}H-NMR (400 MHz, DMSO-d_6): δ 8.19–8.08 (m, 3H), 7.81 (d, J = 24.4 Hz, 2H), 7.60–7.48 (m, 4H), 7.11–7.00 (m, 2H), 6.96 (d, J = 9.3 Hz, 2H), 4.97 (s, 2H), 3.55 (d, J = 5.7 Hz, 3H), 3.33 (d, J = 2.2 Hz, 1H), 3.03 (d, J = 6.1 Hz, 4H); ^{13}C-NMR (101 MHz, DMSO-d_6): δ 173.80, 165.68, 156.27 ($J_{C\text{-}F}$ = 235 Hz), 154.69, 154.66, 147.60 ($J_{C\text{-}F}$ = 2 Hz), 139.23, 134.18, 130.89, 130.46, 128.65 (2C), 128.53 (2C), 125.15, 124.91, 123.33, 118.42, 117.75 ($J_{C\text{-}F}$ = 7 Hz, 2C), 115.31 ($J_{C\text{-}F}$ = 22 Hz, 2C), 69.05, 49.29, 49.00, 44.13, 40.92; ESI-MS *m/z*: Anal. Calcd. for $C_{27}H_{24}FN_2O_4^+$ [M + H]$^+$(459.17), Found: 459.16.

4.5 | 3-(2-(4-(4-Chlorophenyl)Piperazin-1-Yl)-2-Oxoethoxy)-2-Phenyl-4*H*-Chromen-4-One (2d)

White solid, yield 88.6%, m.p. 136.5–137.0°C, ^{1}H-NMR (400 MHz, DMSO-d_6) δ 8.19–8.08 (m, 3H), 7.90–7.75 (m, 2H), 7.57 (d, J = 5.2 Hz, 3H), 7.52 (d, J = 8.0 Hz, 1H), 7.32–7.20 (m, 2H), 7.00–6.91

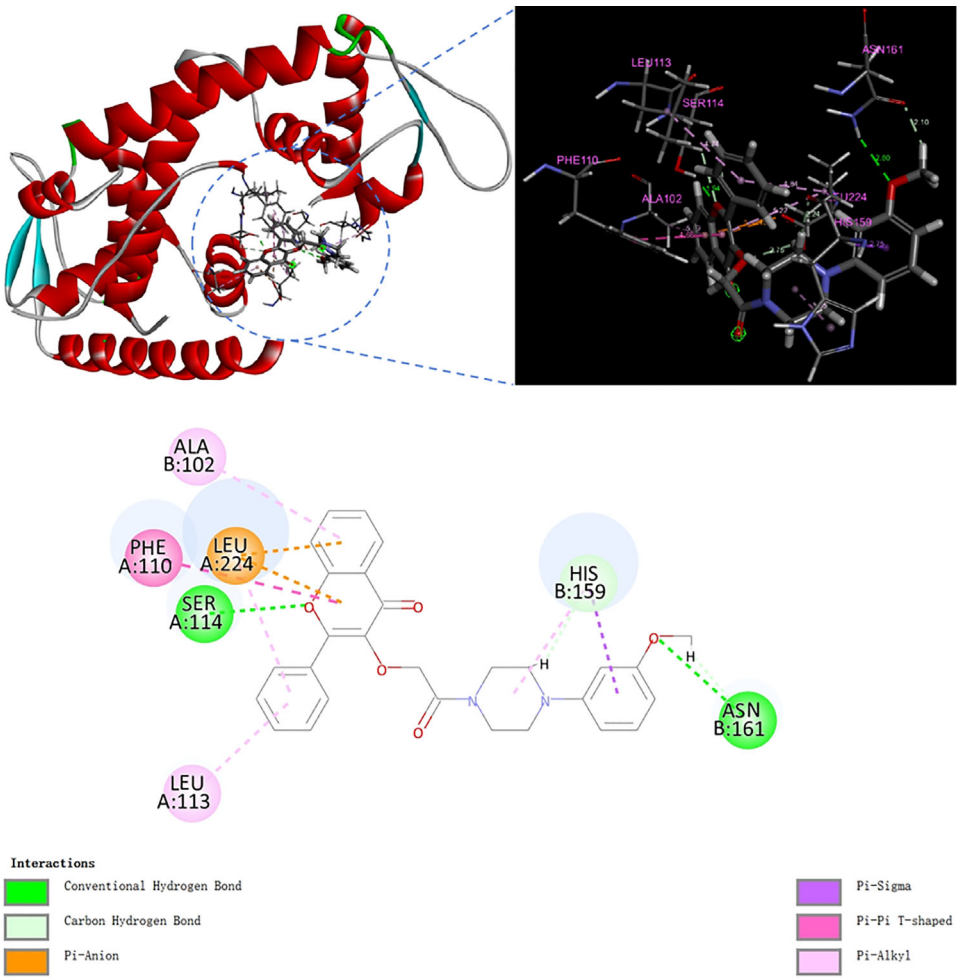

FIGURE 6 | Computer modeling of compound **2g** binding to SarA (2FRH).

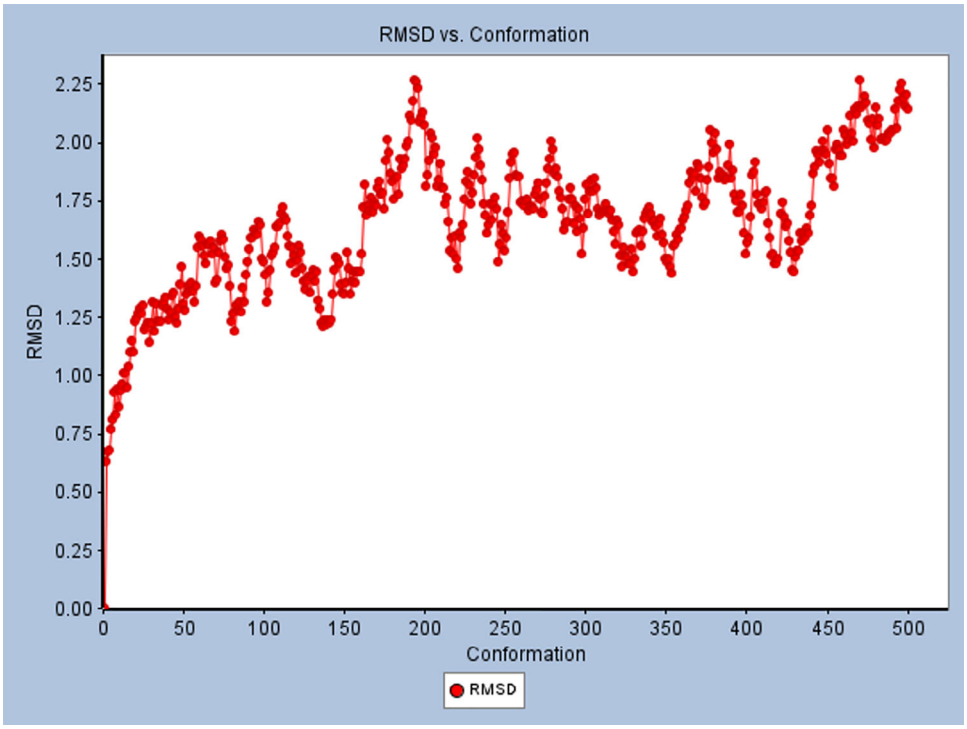

FIGURE 7 | Root-mean-square deviation (RMSD) graph of protein backbone with ligands at 1000 ps simulation (The unit of the vertical axis is Å).

(m, 2H), 4.97 (s, 2H), 3.55 (t, J = 11.2 Hz, 4H), 3.10 (d, J = 5.8 Hz, 4H); ^{13}C-NMR (101 MHz, DMSO-d_6): δ 173.79, 165.72, 154.70, 154.65, 149.49, 139.22, 134.18, 130.88, 130.45, 128.64 (4C), 128.52 (2C), 125.15, 124.91, 123.33, 122.79, 118.42, 117.27 (2C), 69.05, 48.22, 47.90, 43.93, 40.74; ESI-MS *m/z*: Anal. Calcd. for $C_{27}H_{24}ClN_2O_4^+$ [M + H]$^+$(475.14), Found: 475.14.

4.6 | 3-(2-(4-(2,3-Dichlorophenyl)Piperazin-1-Yl)-2-Oxoethoxy)-2-Phenyl-4*H*-Chromen-4-One (2e)

White solid, yield 66.9%, m.p. 129.4–130.0°C, ^{1}H-NMR (400 MHz, DMSO-d_6) δ 8.21–8.12 (m, 2H), 8.11 (d, J = 1.6 Hz, 1H), 7.85 (d, J = 8.6 Hz, 1H), 7.78 (d, J = 8.6 Hz, 1H), 7.59 (d, J = 5.1 Hz, 3H), 7.52 (d, J = 8.1 Hz, 1H), 7.36–7.27 (m, 2H), 7.16–7.07 (m, 1H), 4.98 (s, 2H), 3.61–3.54 (m, 4H), 2.93 (t, J = 4.9 Hz, 4H); ^{13}C-NMR (101 MHz, DMSO-d_6): δ 173.78, 165.81, 154.71, 154.64, 150.65, 139.20, 134.15, 132.60, 130.88, 130.46, 128.67 (2C), 128.53 (2C), 128.46, 126.16, 125.13, 124.90, 124.76, 123.33, 119.83, 118.40, 69.07, 50.97, 50.67, 44.52, 41.23; ESI-MS *m/z*: Anal. Calcd. for $C_{27}H_{23}Cl_2N_2O_4^+$ [M + H]$^+$(509.10), Found: 509.09.

4.7 | 3-(2-(4-(2-Methoxyphenyl)Piperazin-1-Yl)-2-Oxoethoxy)-2-Phenyl-4*H*-Chromen-4-One (2f)

White solid, yield 76.6%, m.p. 142.9–144.0°C, ^{1}H-NMR (400 MHz, DMSO-d_6) δ 8.20–8.14 (m, 2H), 8.12 (d, J = 8.0 Hz, 1H), 7.85 (t, J = 7.7 Hz, 1H), 7.78 (d, J = 8.8 Hz, 1H), 7.58 (d, J = 5.2 Hz, 3H), 7.52 (t, J = 7.5 Hz, 1H), 7.02 - 6.91 (m, 2H), 6.87 (d, J = 5.7 Hz, 2H), 4.97 (s, 2H), 3.79 (s, 3H), 3.55 (d, J = 4.6 Hz, 4H), 2.89 (d, J = 4.7 Hz, 4H); ^{13}C-NMR (101 MHz, DMSO-d_6): δ 173.82, 165.65, 154.67, 154.65, 151.95, 140.68, 139.23, 134.18, 130.89, 130.48, 128.66 (2C), 128.54 (2C), 125.15, 124.92, 123.34, 122.87, 120.79, 118.43, 118.26, 111.84, 69.03, 55.33, 50.23, 49.93, 44.58, 41.30; ESI-MS *m/z*: Anal. Calcd. for $C_{28}H_{27}N_2O_5^+$ [M + H]$^+$(471.19), Found: 471.18.

4.8 | 3-(2-(4-(3-Methoxyphenyl)Piperazin-1-Yl)-2-Oxoethoxy)-2-Phenyl-4*H*-Chromen-4-One (2g)

White solid, yield 70.6%, m.p. 146.3–147.0°C, ^{1}H-NMR (400 MHz, DMSO-d_6) δ 8.18–8.14 (m, 2H), 8.12 (d, J = 8.1 Hz, 1H), 7.85 (d, J = 8.6 Hz, 1H), 7.78 (d, J = 8.6 Hz, 1H), 7.62–7.53 (m, 3H), 7.53-7.48 (m, 1H), 7.12 (t, J = 8.2 Hz, 1H), 6.56-6.49 (m, 1H), 6.46 (t, J = 2.3 Hz, 1H), 6.39 (d, J = 7.8 Hz, 1H), 4.97 (s, 2H), 3.72 (s, 3H), 3.54 (s, 3H), 3.33 (s, 1H), 3.10 (d, J = 5.6 Hz, 4H);^{13}C-NMR (101 MHz, DMSO-d_6): δ 173.80, 165.69, 160.17, 154.68, 154.66, 152.05, 139.23, 134.15, 130.87, 130.45, 129.64, 128.64 (2C), 128.51 (2C), 125.12, 124.90, 123.33, 120.79, 118.40, 104.65, 101.94, 69.07, 54.86, 48.42, 48.13, 44.06, 40.89; ESI-MS *m/z*: Anal. Calcd. for $C_{28}H_{27}N_2O_5^+$ [M + H]$^+$(471.19), Found: 471.18.

4.9 | 3-(2-(4-(4-Methoxyphenyl)Piperazin-1-Yl)-2-Oxoethoxy)-2-Phenyl-4*H*-Chromen-4-One (2 h)

Light yellow solid, yield 75.3%, m.p. 100.2–101.5°C, ^{1}H-NMR (400 MHz, DMSO-d_6) δ 8.17–8.11 (m, 3H), 7.87–7.77 (m, 2H), 7.58–7.50 (m, 4H), 6.90 (d, J = 8.8 Hz, 2H), 6.83 (d, J = 9.2 Hz, 2H), 4.97 (s, 2H), 3.69 (s, 3H), 3.55 (s, 4H), 2.96 (s, 4H);^{13}C-NMR (101 MHz, DMSO-d_6): δ 174.34, 166.18, 155.21, 153.84, 145.60, 139.78, 134.71, 131.42, 131.01, 129.18 (3C), 129.06 (2C), 125.68, 125.45, 123.88, 118.96, 118.57 (2C), 114.78 (2C), 69.60, 55.68, 50.54, 50.29, 44.83, 41.61; ESI-MS *m/z*: Anal. Calcd. for $C_{28}H_{27}N_2O_5^+$ [M + H]$^+$(471.19), Found: 471.13.

4.10 | 3-(2-Oxo-2-(4-(Pyrimidin-2-Yl)Piperazin-1-Yl)Ethoxy)-2-Phenyl-4*H*-Chromen-4-One (2i)

White solid, yield 71.0%, m.p. 139.8–140.0°C, ^{1}H-NMR (400 MHz, DMSO-d_6) δ 8.38 (d, J = 4.8 Hz, 2H), 8.20–8.14 (m, 2H), 8.12 (d, J = 8.0 Hz, 1H), 7.85 (d, J = 8.6 Hz, 1H), 7.78 (d, J = 8.4 Hz, 1H), 7.56 (d, J = 5.3 Hz, 3H), 7.54-7.48 (m, 1H), 6.66 (t, J = 4.8 Hz, 1H), 4.98 (s, 2H), 3.72 (d, J = 7.4 Hz, 4H), 3.48 (t, J = 5.2 Hz, 4H); ^{13}C-NMR (101 MHz, DMSO-d_6): δ 173.78, 165.92, 161.01, 157.94 (2C), 154.69, 154.64, 139.23, 134.14, 130.84, 130.46, 128.65 (2C), 128.49 (2C), 125.11, 124.90, 123.33, 118.40, 110.42, 69.06, 43.89, 43.23, 42.89, 40.78; ESI-MS *m/z*: Anal. Calcd. for $C_{25}H_{23}N_4O_4^+$ [M + H]$^+$(443.17), Found: 443.16.

4.11 | Ethyl 4-(2-((4-Oxo-2-Phenyl-4*H*-Chromen-3-Yl)Oxy)Acetyl)Piperazine-1-Carboxylate (2j)

White solid, yield 85.3%, m.p. 117.0–117.2°C, ^{1}H-NMR (400 MHz, DMSO-d_6) δ 8.20–8.15 (m, 2H), 8.13 (d, J = 8.1 Hz, 1H), 7.86 (d, J = 6.9 Hz, 1H), 7.80 (d, J = 8.6 Hz, 1H), 7.65–7.57 (m, 3H), 7.54 (d, J = 8.1 Hz, 1H), 4.96 (s, 2H), 4.06 (d, J = 8.8 Hz, 2H), 3.42 (d, J = 5.8 Hz, 4H), 3.35 (d, J = 5.5 Hz, 4H), 1.23–1.18 (m, 3H);^{13}C-NMR (101 MHz, DMSO-d_6): δ 173.78, 165.89, 154.70, 154.64, 154.52, 139.20, 134.16, 130.87, 130.45, 128.65 (2C), 128.51 (2C), 125.13, 124.90, 123.31, 118.41, 69.02, 60.90, 54.89, 43.93, 43.17, 40.76, 14.51; ESI-MS *m/z*: Anal. Calcd. for $C_{24}H_{25}N_2O_6^+$ [M + H]$^+$(437.17), Found: 437.17.

4.12 | Benzyl 4-(2-((4-Oxo-2-Phenyl-4H-Chromen-3-Yl)Oxy)Acetyl)Piperazine-1-Carboxylate (2k)

White solid, yield 67.8%, m.p. 125.7–127.0°C, ^{1}H-NMR (400 MHz, DMSO-d_6) δ 8.13 (d, J = 14.5 Hz, 3H), 7.85 (d, J = 8.6 Hz, 1H), 7.81–7.74 (m, 1H), 7.61–7.47 (m, 4H), 7.41-7.28 (m, 5H), 5.10 (s, 2H), 4.94 (s, 2H), 3.44–3.40 (m, 5H), 3.39 (s, 2H), 3.33 (s, 1H); ^{13}C-NMR (101 MHz, DMSO-d_6): δ 173.77, 165.91, 154.71, 154.64, 154.35, 139.20, 136.72, 134.17, 130.86, 130.45, 128.65 (2C), 128.51 (2C), 128.41 (2C), 127.87, 127.60 (2C), 125.14, 124.90, 123.32, 118.41, 69.03, 66.37, 43.92, 43.20, 43.07, 40.76; ESI-MS *m/z*: Anal. Calcd. for $C_{29}H_{27}N_2O_6^+$ [M + H]$^+$(499.19), Found: 499.18.

4.13 | Determination of MIC

The culture medium and the test drug solution were sequentially added to a sterile 96-well plate, ensuring a total volume of 100 μL per well. Subsequently, 100 μL of bacterial suspension (1.5 × 10^6 CFU/mL) was added to each well and mixed thoroughly. The final concentrations of the test compounds in each well were 100, 50, 25, 12.5, 6.25, 3.125, 1.56, 0.78, 0.39, and 0.195 μg/mL, respectively. The 96-well plates were then incubated at 37°C for 24 h in a constant temperature incubator, after which the OD_{600} values were measured using a microplate reader. The

bacterial strains used in the experiments included *S. aureus* ATCC 29213 and *E. coli* ATCC 25922, both of which were obtained from commercial suppliers. Each experimental condition was performed in triplicate.

4.14 | Cytotoxicity Assay

Logarithmic phase L02 cells were harvested and approximately 8,000 cells were seeded into each well of a 96-well plate. The cells were then cultured in a CO_2 incubator at 37°C for 24 h. Subsequently, the culture medium was replaced with test compounds dissolved in dimethyl sulfoxide (DMSO) at concentrations of 0.1, 1, 10, 25, 50, 75, and 100 μM. Six replicates were prepared for each concentration, and a blank control group without test compounds was established. After 48 h of incubation, the supernatant was removed, and 100 μL of cell culture medium containing MTT reagent was added to each well. The plate was incubated in the dark at 37°C for 4 h. Following this, the medium was aspirated, and 150 μL of DMSO was added to dissolve the formazan crystals. The plate was shaken gently on a shaker at low speed for 15 min, and the absorbance of each well was measured at 490 nm using a microplate reader. Finally, the IC_{50} value was calculated based on the obtained data.

4.15 | The Oxford Cup Method for Assessing Compound Antibacterial Effects

In a laminar flow hood, 100 μL of bacterial suspensions of *S. aureus* and *E. coli* (1.5×10^6 CFU/mL) were separately inoculated onto two sterile agar plates. Then, they were spread three times evenly with a sterile cotton swab, rotating the plate 60° each time, and spreading along the edge of the plate in a circular motion. A sterilized Oxford cup was carefully placed on the inoculated medium using sterile forceps to ensure complete contact with the surface. Each cup received 200 μL of the test compound at a concentration of 8 × MIC, while an equal volume of solvent served as the negative control. The plates were incubated at 37°C in a constant temperature incubator for 24 h. Following incubation, the diameters of the inhibition zones were measured, and the entire experiment was repeated in triplicate.

4.16 | Time-Kill Kinetics Experiment

Single colonies of *S. aureus* and *E. coli*, which had been previously subcultured, were separately inoculated into brain heart infusion (BHI) agar medium and incubated at 37°C in a constant temperature shaking incubator for 16-18 h. The bacterial suspensions were then adjusted to a concentration of 1.5×10^6 CFU/mL using sterile broth. Test compounds were dissolved in DMSO and subsequently diluted with distilled water to prepare stock solutions with a final concentration of 8 times the MIC for subsequent use.

Twenty-one sterile 5 mL tubes were prepared and labeled for the negative control group, sample group, and positive control group at time points of 0, 0.5, 1, 2, 4, 8, and 24 h. The negative control group was prepared by combining 1 mL of bacterial suspension with 1 mL of broth medium. For the sample group, 1 mL of bacterial suspension was mixed with 1 mL of an 8 × MIC test compound solution. The positive control group was prepared by mixing 1 mL of bacterial suspension with 1 mL of an 8 × MIC levofloxacin solution. All tubes were incubated at 37°C. At each designated time point (0.5, 1, 2, 4, 8, and 24 h), 100 μL aliquots were taken from each tube and serially diluted in fresh sterile broth medium to achieve dilutions ranging from 10^{-1} to 10^{-7}. Each dilution was then spread on agar plates, which were incubated at 37°C for 24 h. Plates containing colony counts between 30 and 300 colonies were selected for enumeration. The experiment was replicated twice.

4.17 | Effects of Compound 2g on Biofilms

In a laminar flow hood, 100 μL of compound **2g** at a concentration of 8 × MIC and 100 μL of *S. aureus* bacterial suspension were added to each well of a 96-well plate. An equal volume of BHI served as the blank control group, with three replicates for each condition. The plates were incubated at 37°C for 4 h, 20 h, and 24 h. Following incubation, the supernatant was carefully aspirated from each well, and the wells were gently washed three times with sterile distilled water. Subsequently, 200 μL of crystal violet staining solution was added to each well and incubated at room temperature for 15 min. Excess stain was discarded, and the wells were rinsed three times with sterile distilled water before being allowed to air dry. Finally, 30% acetic acid solution was added to each well and incubated for 20 min to dissolve the bound stain. The OD_{570} value was measured using a microplate reader.

4.18 | Molecular Docking and Molecular Dynamics Simulation Experiments

Molecular docking simulations were conducted using Discovery Studio (DS) 2021 software. The protein and ligand structures were preprocessed by removing water molecules, adding hydrogen atoms via the DS Server, and preparing the samples for docking analysis. The docking calculations were performed and analyzed using DS-Client. Specifically, the crystal structure of SarA (PDB ID: 2FRH) [26] was selected as the target protein for this study. The binding site was defined as a sphere centered at the XYZ coordinates (-0.1483, -18.0931, and 29.2759) with a radius of 8.3 Å. The LibDock protocol was employed to perform the docking studies. The resulting ligand poses were evaluated based on their LibDockScore values.

The molecular dynamics simulations were conducted using DS software version 2021. The protein-ligand complexes obtained from the aforementioned molecular docking studies were imported into DS software. The CHARMM36 force field was employed to generate the protein topology file, and the system was solvated using the default TIP3P water model in a cubic box to mimic physiological conditions. Subsequently, counterions (Na^+ or Cl^-) were added to neutralize the system charge. Production molecular dynamics simulations were performed for 1000 ps with the CHARMM36 force field and a time step of 2 fs. The resulting trajectories were analyzed to calculate the RMSD of the protein-ligand complexes and assess their conformational stability (Supporting Information).

Author Contributions

Jin Wang, **Si-Jiao Cui**, and **Jia-Xin Liu** were responsible for the synthesis and identification of the compounds; **Xin-Ming Li** and **Da-Jun Zhang** conducted the biological experiments; **Tian Luan** designed and drafted the manuscript. All authors contributed to data analysis and discussion. All authors have reviewed the final manuscript and approved its submission.

Acknowledgments

This study received funding from the Scientific Research Project of the Department of Education of Liaoning Province, China (No. JYTMS20231407) and the Project of Science and Technology Department of Liaoning Province, China (No. 2024-MS-226; No. 2023-MS-328).

Conflicts of Interest

The authors declare no conflicts of interest.

Data Availability Statement

The Supporting Information contains the data underpinning the conclusions of this study.

References

1. S. Gandra, K. K. Tseng, A. Arora, et al., "The Mortality Burden of Multidrug-resistant Pathogens in India: A Retrospective, Observational Study," *Clinical Infectious Diseases* 69 (2019): 563–570.

2. G. Ahmad, A. Khalid, M. U. Qamar, et al., "Antibacterial Efficacy of N-(4-methylpyridin-2-yl) Thiophene-2-Carboxamide Analogues Against Extended-Spectrum-β-Lactamase Producing Clinical Strain of Escherichia coli ST 131," *Molecules* 28, no. 7 (2023): 3118.

3. A. H. Khan, M. Bilal, A. Mahmood, et al., "Facile Synthesis of N-(4-Bromo-3-methylphenyl)pyrazine-2-carboxamide Derivatives, Their Antibacterial Activities Against Clinically Isolated XDR S. Typhi, Alkaline Phosphatase Inhibitor Activities, and Docking Studies," *Pharmaceuticals* 17, no. 9 (2024): 1241.

4. S. Naheed, I. U. Din, M. U. Qamar, et al., "Synthesis, Anti-Bacterial and Molecular Docking Studies of Arylated Butyl 2-Bromoisonicotinate against Clinical Isolates of ESBL-Producing Escherichia coli ST405 and Methicillin-Resistant Staphylococcus aureus," *Infection and Drug Resistance* 16 (2023): 5295–5308.

5. M. Noreen, M. Bilal, M. Usman Qamar, et al., "Facile Synthesis of 5-Bromo-N-Alkylthiophene-2-Sulfonamides and Its Activities against Clinically Isolated New Delhi Metallo-β-Lactamase Producing Klebsiella pneumoniae ST147," *Infection and Drug Resistance* 17 (2024): 2943–2955.

6. G. D. Hatnapure, A. P. Keche, A. H. Rodge, S. S. Birajdar, R. H. Tale, and V. M. Kamble, "Synthesis and Biological Evaluation of Novel Piperazine Derivatives of Flavone as Potent Anti-inflammatory and Antimicrobial Agent," *Bioorganic & Medicinal Chemistry Letters* 22 (2012): 6385–6390.

7. M. D. Burton, J. L. Rytych, R. Amin, and R. W. Johnson, "Dietary Luteolin Reduces Proinflammatory Microglia in the Brain of Senescent Mice," *Rejuvenation Research* 19 (2016): 286–292.

8. M. J. Yousefzadeh, Y. Zhu, S. J. McGowan, et al., "Fisetin Is a Senotherapeutic That Extends Health and Lifespan," *EBioMed* 36 (2018): 18–28.

9. M. Siah, M. H. Farzaei, M. R. Ashrafi-Kooshk, et al., "Inhibition of guinea Pig Aldehyde Oxidase Activity by Different Flavonoid Compounds: An in Vitro Study," *Bioorganic Chemistry* 64 (2016): 74–84.

10. J. Johari, A. Kianmehr, M. Mustafa, S. Abubakar, and K. Zandi, "Antiviral Activity of Baicalein and Quercetin Against the Japanese Encephalitis Virus," *International Journal of Molecular Sciences* 13 (2012): 16785–16795.

11. M. Friedman, "Overview of Antibacterial, Antitoxin, Antiviral, and Antifungal Activities of Tea Flavonoids and Teas," *Molecular Nutrition & Food Research* 51 (2006): 116–134.

12. X. Han, T. Xu, Q. Fang, et al., "Quercetin Hinders Microglial Activation to Alleviate Neurotoxicity via the Interplay Between NLRP3 Inflammasome and Mitophagy," *Redox Biology* 44 (2021): 102010.

13. Y. Wu, J. Chen, W. Wei, et al., "A Study of the Antibacterial Mechanism of Pinocembrin Against Multidrug-resistant Aeromonas Hydrophila," *International Microbiology* 25 (2022): 605–613.

14. T. L. A. Nguyen and D. Bhattacharya, "Antimicrobial Activity of Quercetin: An Approach to Its Mechanistic Principle," *Molecules* 27 (2022): 2494.

15. S. Wang, J. Yao, B. Zhou, et al., "Bacteriostatic Effect of Quercetin as an Antibiotic Alternative In Vivo and Its Antibacterial Mechanism In Vitro," *Journal of Food Protection* 81 (2018): 68–78.

16. Q.-H. Wen, R. Wang, S.-Q. Zhao, B.-R. Chen, and X.-A. Zeng *Foods* (2021): 10.

17. X. Li, C. He, L. Song, et al., "Antimicrobial Activity and Mechanism of Larch Bark Procyanidins Against *Staphylococcus aureus*," *Acta Biochim Biophys Sin* 49 (2017): 1058–1066.

18. H. Liang, K. He, T. Li, et al., "Mechanism and Antibacterial Activity of Vine Tea Extract and Dihydromyricetin Against *Staphylococcus aureus*," *Scientific Reports* 10 (2020): 21416.

19. G. Gutiérrez-Venegas, J. A. Gómez-Mora, M. A. Meraz-Rodríguez, M. A. Flores-Sánchez, and L. F. Ortiz-Miranda, "Effect of Flavonoids on Antimicrobial Activity of Microorganisms Present in Dental Plaque," *Heliyon* 5 (2019): e03013.

20. X.-Y. Shi, H. Jiao, J.-K. Zhang, et al., "Discovery of Novel Arylamide Derivatives Containing Piperazine Moiety as Inhibitors of Tubulin Polymerisation With Potent Liver Cancer Inhibitory Activity," *Journal of Enzyme Inhibition and Medicinal Chemistry* 38 (2023): 2237701.

21. R. B. Clark, D. Lamppu, L. Libertine, et al., "Discovery of Novel 2-((Pyridin-3-yloxy)Methyl)Piperazines as α7 Nicotinic Acetylcholine Receptor Modulators for the Treatment of Inflammatory Disorders," *Journal of Medicinal Chemistry* 57 (2014): 3966–3983.

22. A. F. Brito, L. K. S. Moreira, R. Menegatti, and E. A. Costa, "Piperazine Derivatives With Central Pharmacological Activity Used as Therapeutic Tools," *Fundamental and Clinical Pharmacology* 33 (2018): 13–24.

23. E. Lacivita, M. Leopoldo, P. D. Giorgio, F. Berardi, and R. Perrone, "Determination of 1-Aryl-4-Propylpiperazine pKa Values: The Substituent on Aryl Modulates Basicity," *Bioorganic & Medicinal Chemistry* 17 (2009): 1339–1344.

24. E. Kovács, B. Rózsa, A. Csomos, I. G. Csizmadia, and Z. Mucsi, "Amide Activation in Ground and Excited States," *Molecules* 23 (2018): 2859.

25. D. A. Brown, P. S. Kharkar, I. Parrington, M. E. A. Reith, and A. K. Dutta, "Structurally Constrained Hybrid Derivatives Containing Octahydrobenzo[g or f]Quinoline Moieties for Dopamine D2 and D3 Receptors: Binding Characterization at D2/D3 Receptors and Elucidation of a Pharmacophore Model," *Journal of Medicinal Chemistry* 51 (2008): 7806–7819.

26. Y. Liu, A. C. Manna, C.-H. Pan, et al., "Structural and Function Analyses of the Global Regulatory Protein SarA From *Staphylococcus aureus*," *PNAS* 103 (2006): 2392–2397.

Supporting Information

Additional supporting information can be found online in the Supporting Information section.